

MonoIR-RS: Infrared Remote Sensing Vision-Language Learning with CLIP and VLM Adaptation

Jiaju Han^{1,3}, Ma Yaqi², Yahui Chai¹, Xuemeng Sun¹, Xin Li¹, Qike Zhang¹, Yingying Zhao¹, Xiang Chen¹, Luwei Yang³, Chengyin Hu¹, and Jiahuan Long⁴

¹ China University of Petroleum-Beijing at Karamay, Karamay, Xinjiang, China

² Guizhou University, Guiyang, China

³ Shenzhen Research Institute of Big Data, Shenzhen, China

⁴ Shanghai Jiao Tong University, Shanghai, China

Abstract. Infrared remote-sensing imagery captures intensity structure, object-background contrast, and illumination-invariant cues often invisible in RGB imagery. Yet, most remote-sensing vision-language resources and models focus on visible-band semantics, leaving infrared vision-language understanding underexplored. We introduce MonoIR-RS, a large-scale infrared remote-sensing vision-language dataset and benchmark that couples IR-aware data construction with CLIP-style contrastive adaptation and VLM instruction tuning. Built from the same source pool and split as FusionRS, MonoIR-RS retains only the infrared image as the model-facing modality, yielding 600,000 synthesized infrared images and 59,032 retained IR-aware caption records. The model experiments use this retained language-supervision subset, whose captions rewrite supervision around grayscale structure and infrared-style contrast instead of RGB appearance. We show that the synthesized infrared is markedly closer to real thermal imagery than a grayscale conversion on the AVIID benchmark. We fine-tune five CLIP backbones and six VLM backbones, and calibrate them against zero-shot behavior: IR-aware adaptation lifts CLIP mean recall by up to +12.8 points (best checkpoint 19.2% on the 9,720-image filtered split) and drives VLM captioning IR-cue coverage to 100% while reducing residual RGB-color leakage to near zero. By isolating the infrared modality from RGB-IR dual-modal learning, MonoIR-RS offers a controlled, reproducible testbed for aligning infrared remote-sensing evidence with language.

Keywords: Infrared remote sensing · Vision-language learning · CLIP fine-tuning · Visual instruction tuning · Dataset evaluation

1 Introduction

Infrared remote sensing is important for visual understanding under illumination changes, low-visibility conditions, and intensity contrast not captured by

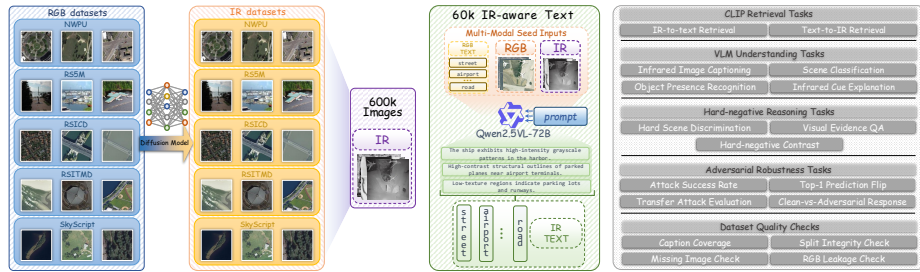


Fig. 1: Overview of the MonoIR-RS construction workflow. The shared FusionRS source pool is converted into an infrared image-text corpus, IR-aware text, and evaluation tasks covering retrieval, VLM understanding, and dataset-quality checks.

visible-band imagery, where discriminative evidence includes object-background separation and grayscale response rather than color. This makes infrared imagery valuable for nighttime monitoring, fire observation, and low-visibility analysis, yet difficult to serve with vision-language models trained on RGB web photography. The gap goes beyond a domain shift: infrared and visible sensors register the same scene under different physical principles, so captions written for visible images frequently describe color cues that are absent or misleading in the infrared modality.

Recent vision-language models, including CLIP-style contrastive models and instruction-following VLMs, have made remote-sensing retrieval, captioning, and question answering more practical. RemoteCLIP and GeoRSCLIP show that domain-specific supervision improves remote-sensing representations, while GRAFT aligns satellite and ground-level imagery without direct text annotations [18, 23, 35], and remote-sensing VLMs extend this toward grounded dialogue and geospatial benchmarking [9, 16, 36]. Infrared-specific efforts such as Infrared-LLaVA and IRGPT have begun to address the modality gap, but they target general surveillance or pedestrian infrared rather than remote sensing and rely on real sensor captures that are scarce and expensive to scale [6, 15]. Transfer to infrared remote sensing therefore faces three bottlenecks: image-text resources are dominated by visible images; infrared captions must describe thermal evidence and grayscale structure rather than RGB appearance; and fair evaluation requires clean category protocols and strict split hygiene, since mixed phrases, residual RGB paths, or loose candidate pools can inflate conclusions.

This paper tackles infrared remote-sensing vision-language learning as an integrated data, adaptation, and evaluation problem. We build an IR-aware data pipeline that synthesizes infrared imagery from visible remote-sensing sources via diffusion and rewrites supervision around infrared-style visual evidence, fine-tune five CLIP and six VLM backbones under a train-only protocol, and evaluate against zero-shot behavior where the comparison is available. Rather than claiming photorealism, we validate the synthetic modality directly: it is closer to real thermal imagery than a grayscale conversion under both FID and histogram distance against the AVIID benchmark. As an auxiliary transfer sanity check, an

IR-aware fine-tuned CLIP retrieves matching visible images from real infrared queries +6.5 mean-recall points better than its zero-shot counterpart on AVIID; this check is separate from the main infrared benchmark. This unified view (Fig. 1) lets us test whether IR-aware supervision benefits both retrieval models and VLMs under one data boundary, and whether gains survive controlled candidates, split audits, and per-source diagnosis. Our contributions follow.

- We propose MonoIR-RS, a large-scale infrared remote-sensing vision-language dataset and benchmark with 600,000 synthetic infrared images and 59,032 retained IR-aware caption records supervised around infrared-style visual evidence. Validated against the real AVIID benchmark, its synthetic modality is closer to real infrared than a grayscale conversion by both FID and histogram distance.
- We adapt five CLIP and six VLM backbones under a train-only protocol, calibrating each family against zero-shot behavior. IR-aware CLIP adaptation yields +3.5 to +12.8 mean-recall gains (best 19.2%), with a seed-stability check on OpenAI CLIP ViT-B/32, and transfers to real-infrared image retrieval on AVIID.
- We show that fine-tuning drives VLM captioning IR-cue coverage to 100% while reducing RGB-color leakage relative to zero-shot models. Five diagnostic metrics—IR-cue rate, color-leakage rate, overclaim rate, class-hit rate, and response length—capture complementary failure modes that no single metric summarizes.

2 Related Work

2.1 Vision-Language Learning for Remote Sensing

Remote-sensing vision-language learning has expanded from image classification toward retrieval, captioning, grounding, and multimodal reasoning, with CLIP-style contrastive learning aligning image-text embeddings and VLMs extending to free-form instructions. RemoteCLIP builds a remote-sensing foundation model from large-scale image-text supervision [18]; RS5M and GeoRSCLIP scale the dataset and model for retrieval and zero-shot recognition [35]; GRAFT aligns satellite with ground-level imagery to reduce annotation dependence [23]; and longer-text and transductive methods further refine image-text matching [7, 33].

GeoChat studies grounded remote-sensing dialogue [16]. SkySense and SkySense-O address open-world Earth observation interpretation [10, 36]. EarthDial, GEOBench-VLM, and large-image VLM work cover dialogue, benchmarking, and token handling [9, 22, 28]. These efforts advance RGB and multi-sensor remote-sensing VLMs, but do not isolate the infrared setting, where color descriptions are unreliable and thermal evidence should guide supervision.

2.2 Infrared and Thermal Remote-Sensing Data

Infrared remote-sensing data differ from RGB in sensing physics and visual semantics: intensity contrast, sensor artifacts, and missing color make captions

Table 1: Comparison with related datasets by modality, scale, domain, and primary use. The final row highlights the infrared vision-language setting of MonoIR-RS, in contrast to dual-modal RGB-IR resources and RGB-only remote-sensing image-text datasets.

Dataset	Modality	Scale	Domain	Primary use / limitation
LLVIP [14]	RGB-IR	15K pairs	Low-light surveillance	Detection / fusion; no language
M3FD [20]	RGB-IR	4K pairs	Street scenes	Fusion / detection; non-RS
MFNet [11]	RGB-thermal	1.6K pairs	Urban driving	Segmentation; no language
VEDAI [26]	Multi-spectral	1.2K images	Aerial vehicles	Detection; no language
DroneVehicle [29]	UAV RGB-IR	28K pairs	UAV traffic	Detection; no caption/VQA
RSICD [21] / RSITMD [32]	RGB-text	10.9K / 4.7K	Remote sensing	Caption/retrieval; RGB-only
RS5M / GeoRSCLIP [35]	RGB-text	5M pairs	Remote sensing	CLIP pretraining; RGB-only
SkyScript [30]	RGB-text	2.6M pairs	Remote sensing + OSM	VLM data; RGB-only
IRGPT / IR-TD [6]	IR-text	260K pairs	General infrared	IR language; non-RS
FireMM-IR [4]	RGB-IR + instr.	task-specific	Forest-fire RS	Dual-modal; scenario-specific
FusionRS [12]	RGB-IR-text	600K triplets	General remote sensing	Dual-modal RGB-IR CLIP/VLM training
MonoIR-RS (ours)	IR-text + instr.	600K IR images / 59K caption records	General remote sensing	Infrared CLIP/VLM fine-tuning

like “green field” or “blue roof” inappropriate for infrared scenes, so IR vision-language datasets need IR-aware text, not RGB captions copied onto infrared images. Table 1 positions MonoIR-RS against nearby RGB-IR, infrared, and remote-sensing vision-language resources.

Existing efforts span spectral and multi-modal Earth observation. S2MAE studies spatial-spectral pretraining for spectral RS [17], AnySat targets multiple resolutions and modalities [1], and Infrared-LLaVA adapts MLLMs to infrared understanding [15]. Most relevant, IRGPT [6] builds a large real-infrared corpus and argues synthetic IR introduces a modality gap. We differ: IRGPT targets general IR (surveillance, pedestrian) with text produced by an LLM from the paired *visible* image, whereas we target remote-sensing IR with supervision rewritten around infrared evidence; and we adopt DiffV2IR [25], whose visible-to-infrared translation attains strong fidelity (low FID/PSNR/SSIM against real thermal benchmarks), and validate the modality against real infrared directly (Sec. 3). Per the synthetic-data literature, we treat downstream utility, not photorealism, as the bar.

2.3 Fine-Tuning CLIP and VLM Backbones

Fine-tuning pretrained CLIP improves alignment for domain-specific image-text pairs, while VLM instruction tuning adapts multimodal assistants to specialized questions and scene descriptions. Domain prompt learning and controlled CLIP-transfer studies show that data distribution and adaptation strategy strongly affect downstream behavior, and that scaling data without quality control can degrade representations [5, 31]. Visual instruction tuning is now the standard route for adapting VLMs [19], with work on data selection, compact visual tokens, and low-rank adaptation [3, 27, 34]. These methods compare heterogeneous backbones under a shared training budget, which is essential when the contribution lies in data and protocol rather than one model.

For infrared remote sensing, CLIP and VLM fine-tuning play different roles: CLIP targets compact retrieval and embedding-space alignment, while VLMs target instruction following, captioning, and evidence-grounded QA. Our pipeline

Table 2: Distance to real infrared (AVIID, 804 test images). Synthetic infrared from DiffV2IR is compared with a direct RGB-to-gray baseline over Inception FID and grayscale-histogram metrics; lower is closer for FID/KL/JS/ χ^2 , higher for histogram intersection.

vs. Real IR	FID ↓	KL ↓	JS ↓	χ^2 ↓	Hist. inter. ↑
Synthetic IR (DiffV2IR)	85.2	0.103	0.027	0.051	0.822
RGB-to-gray baseline	126.3	0.545	0.079	0.139	0.711

separates the two families and couples both with data-integrity diagnostics, so gains are judged by task scores and by whether they survive controlled candidate pools, split audits, and zero-shot calibration.

3 Dataset Description

3.1 Data Sources and Construction Goal

MonoIR-RS targets infrared remote-sensing vision-language training rather than dual-modal RGB-IR inference. It follows the same source pool and sample-level split as FusionRS but changes the modeling target: each sample exposes only the infrared image to the model, while the visible image is retained only for construction-time alignment and auditing. This isolates the infrared modality, where scene understanding must rely on grayscale structure, intensity contrast, and object-background separation rather than color. As shown in Tables 3 and 4, the corpus contains 600,000 infrared samples from five sources and 59,032 IR-aware caption records after filtering. The image pool and the retained language-supervision subset are reported separately: not every synthesized infrared image contributes a retained caption after filtering, and the reported CLIP/VLM experiments use only retained train-split language supervision. RS5M and SkyScript provide large-scale coverage, while NWPU, RSICD, and RSITMD add established scene categories and fine-grained benchmark examples. The retained records are normalized into a unified infrared image-text format, supporting CLIP contrastive fine-tuning, VLM instruction tuning, and controlled evaluation under one split protocol. Figure 2 previews the resulting task formats.

Because the five source collections provide only visible-band imagery, the infrared modality is synthesized rather than sensor-captured. We generate each infrared image from its registered visible image with DiffV2IR [25], a visible-to-infrared diffusion model that couples a progressive full-range-to-target-wavelength learning module with vision-language guidance and is trained on a large infrared image collection. This yields infrared-style renderings whose grayscale structure, object-background contrast, and thermal-response layout follow the source scene while removing color cues. We treat these renderings as a controlled, reproducible infrared testbed for vision-language adaptation rather than as radiometrically calibrated sensor measurements. This construction choice motivates

Table 3: Infrared split derived from the shared FusionRS source pool after retaining only model-facing IR images.

Source	Total	Train	Val	Test
RS5M [35]	488,033	471,729	8,166	8,138
SkyScript [30]	65,266	63,134	1,036	1,096
NWPU [8]	31,186	30,122	549	515
RSICD [21]	10,824	10,494	166	164
RSITMD [32]	4,691	4,521	83	87
Total	600,000	580,000	10,000	10,000

Table 4: Distribution of IR-aware caption records across splits after filtering RGB-dependent, empty, and invalid entries.

Split	Records	Model use
Train	48,616	CLIP training / VLM source pool
Val	416	Checkpoint selection
Test	10,000	Held-out evaluation
Total	59,032	Train/val/test captions

our IR-aware supervision and RGB-leakage audits, since color words carried over from the source captions are unsupported by the synthesized infrared evidence.

To check that the synthesized modality is closer to real infrared than a naive grayscale conversion, we compare against the real aerial visible-infrared dataset AVIID [13]. We render synthetic infrared from its 804 visible test images with the same DiffV2IR pipeline and compare the synthetic infrared, the real infrared, and a direct RGB-to-gray conversion (Table 2). By both FID and all four grayscale-histogram metrics, the synthetic infrared is markedly closer to real infrared than the grayscale baseline (FID 85.2 vs. 126.3). DiffV2IR thus captures infrared intensity structure beyond simple desaturation, though we still treat it as an infrared-like approximation, not a radiometrically calibrated sensor substitute.

Beyond distributional similarity, we run an auxiliary paired image-image retrieval sanity check on AVIID to test whether synthetic-IR adaptation transfers to real-infrared inputs. Using the selected IR-CLIP checkpoint, real-IR queries retrieve visible targets with 18.7% mean recall, a +6.5-point gain over the corresponding zero-shot CLIP (12.2%); with synthetic-IR queries against real-IR targets, the gain is +23.4 points. This experiment is not part of the main infrared benchmark itself, but it tests whether the learned infrared representation carries signal beyond the synthetic training domain.

3.2 IR-Aware Text Generation

Source captions often contain color words or visible-band details unreliable in infrared imagery, so we rewrite supervision to emphasize grayscale structure, thermal contrast, and scene layout. IR-aware captions are generated with Qwen2.5-VL-72B-Instruct [2] from the source text and infrared evidence, preserving scene semantics while replacing RGB-dependent descriptions with infrared-grounded cues and discouraging unsupported color terms. Table 4 summarizes the subset after filtering empty outputs, weak descriptions, unsupported claims, missing images, and invalid split entries. The retained supervision serves two formats: image-text pairs for CLIP contrastive fine-tuning and a train-only source pool from which VLM instruction-answer examples are constructed.

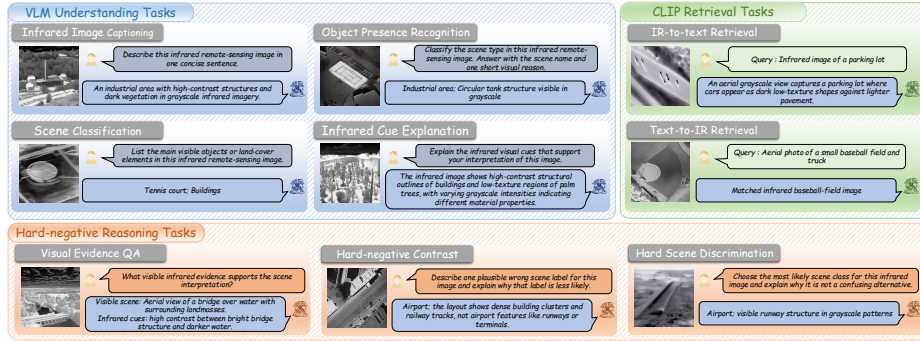


Fig. 2: Representative MonoIR-RS task formats derived from infrared remote-sensing supervision, including VLM understanding, CLIP retrieval, and visual-evidence QA with paired prompts and target responses.

3.3 Split Hygiene and Quality Control

We constrain all fine-tuning data to the train split; validation and test images are excluded before CLIP or VLM training, and empty or non-train entries are treated as invalid. This shared boundary adapts both model families under the same train-only protocol, preventing hidden differences between the contrastive and instruction-tuning stages. We also keep dataset-integrity checks in the release surface: split-overlap auditing, missing-image checks, duplicate-path inspection, and RGB-leakage inspection, since residual visible-band paths or mixed entries can overstate infrared generalization. The original test split has 10,000 samples; the formal filtered surface retains 9,720 after flagging 280 RGB-named paths.

4 CLIP and VLM Model Fine-Tuning

4.1 Overview

The model adaptation pipeline has two stages, as illustrated in Fig. 3. The first fine-tunes CLIP-style encoders for infrared-text contrastive alignment; the second adapts VLM backbones for instruction-style infrared understanding. We use fine-tuning rather than from-scratch pretraining to test how existing vision-language priors can be redirected toward infrared evidence under a controlled data boundary, keeping backbone capacity fixed so the effect of IR-aware supervision is comparable across models. The two stages are intentionally separated: CLIP provides compact embeddings for retrieval, whereas VLMs generate free-form answers for captioning, visual-evidence QA, object recognition, and infrared-cue explanation. This matters because retrieval alignment does not guarantee reliable instruction following, and fluent generation does not guarantee correct infrared grounding. Both stages use only train-split infrared images and IR-aware supervision.

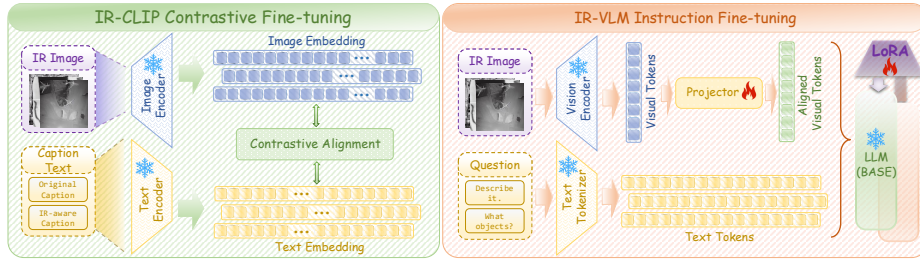


Fig. 3: Two-stage model adaptation used for MonoIR-RS. The left branch fine-tunes CLIP-style encoders with infrared image-text contrastive alignment, while the right branch adapts VLM backbones with infrared visual tokens, a projector, and LoRA-based instruction tuning.

4.2 Training Data Interface

The same infrared source boundary is exposed to the two model families through different interfaces. For CLIP, each retained train record is an image-text pair (I_{ir}, t_{ir}) , matching the bidirectional retrieval objective used in evaluation. For VLMs, train-split records are converted and filtered into instruction triples (I_{ir}, q, a) , where q may request captioning, scene recognition, object presence, or infrared-cue explanation. The final VLM recipe uses the API-v3 multitask subset of 32,000 conversations selected from the train split, rather than all 48,616 retained train captions. RGB images stay outside the model-facing path, used only as construction-time alignment evidence. The two stages thus share one data discipline: train-only optimization and no use of held-out evaluation images during adaptation.

4.3 IR-CLIP Contrastive Fine-Tuning

For IR-CLIP fine-tuning, the image encoder maps the infrared input into a visual embedding, the text encoder maps the IR-aware caption into a language embedding, and a symmetric contrastive objective aligns matched pairs while separating in-batch negatives. This adapts pretrained vision-language priors to infrared remote sensing without relying on RGB appearance, where the visual evidence is dominated by grayscale layout, thermal contrast, sensor-specific texture, and fine structural boundaries. We evaluate five CLIP backbones spanning general and remote-sensing variants. During fine-tuning, the text side is frozen and the visual tower plus projection layers are adapted, so the main optimization pressure falls on aligning infrared evidence to the existing language space while preserving stable text semantics. Checkpoints are selected by validation mean recall and used for bidirectional IR-text retrieval.

4.4 IR-VLM Instruction Fine-Tuning

For IR-VLM fine-tuning, each example contains an infrared image, an instruction, and a target answer derived from IR-aware supervision. The vision encoder

Table 5: Training configuration for IR-CLIP and IR-VLM fine-tuning. Backbones are listed together within each family, while shared trainable modules, objectives, schedules, and checkpoint-selection rules are reported once per family.

Field	Configuration
IR-CLIP family — contrastive IR image-text fine-tuning	
Backbones	OpenAI CLIP ViT-B/32, OpenAI CLIP ViT-L/14, OpenCLIP ViT-B/32, RemoteCLIP ViT-B/32, GeoRSCLIP ViT-B/32
Trainable / objective	Visual tower and projection layers; text encoder frozen; contrastive IR image-text alignment
Schedule	2 epochs; batch size 768 (OpenAI B/32), 128 (OpenAI L/14), 1024 (OpenCLIP, RemoteCLIP, GeoRSCLIP); learning rate 2×10^{-6} for B/32-family backbones and 1×10^{-6} for OpenAI L/14
Selection	Best checkpoint by validation mean recall
IR-VLM family — instruction-style infrared understanding	
Backbones	Qwen2.5-VL-7B [2], InstructBLIP-FLAN-T5-XL, LLaVA-1.5-7B [19], LLaVA-1.6-Vicuna-7B, GeoChat-7B [16], H2RSVLM-VHM-7B [24]
Trainable / objective	LoRA adapters ($r = 32$, $\alpha = 64$, dropout 0.05) and trainable multimodal projector where exposed by the backbone; base LLM frozen; instruction-following loss
Schedule	1 epoch; batch/accum. 1×8 (Qwen), 2×8 (InstructBLIP), 4×4 (LLaVA, GeoChat, H2RSVLM); learning rate 2×10^{-4} , cosine schedule, 0.03 warmup ratio
Selection	Final-epoch adapter; save-total-limit 1

extracts infrared visual tokens, a projector maps them into the language-model embedding space when the backbone exposes a trainable projector, and LoRA adapters update instruction-following behavior while keeping the base language model frozen. This parameter-efficient setting makes it feasible to compare heterogeneous VLM backbones under a common infrared interface and reduces confounding from full-model optimization. The instruction data cover complementary forms of infrared understanding: captioning prompts summarize global scene structure, scene and object prompts encourage short semantic decisions, and infrared-cue or visual-evidence prompts require answers grounded in grayscale layout, object-background contrast, thermal evidence, and observable scene geometry.

4.5 Training Configuration

Table 5 reports the training configuration for the two model families: CLIP uses contrastive alignment with a frozen text encoder, and VLMs use parameter-efficient instruction tuning with LoRA adapters and projector tuning where applicable. The settings keep each family within a standard regime while preserving the same data boundary and evaluation protocol. CLIP checkpoints are selected by validation mean recall; for VLMs we retain the final-epoch adapter under a

Table 6: Clean IR-CLIP retrieval on the 9,720-image filtered infrared test split. All values are percentages; mR averages R@1, R@5, and R@10 for both retrieval directions. The final two columns compare zero-shot mR (original pretrained weights, no IR-aware fine-tuning) with our fine-tuned mR, and Δ is the absolute gain from IR-aware adaptation.

Model	I2T R@1	I2T R@5	I2T R@10	T2I R@1	T2I R@5	T2I R@10	Zero-shot mR	mR	Δ
OpenAI CLIP ViT-L/14	8.3	19.8	27.1	9.5	21.4	28.8	6.3	19.2	+12.8
GeoRSCLIP ViT-B/32	5.3	14.1	20.4	5.6	14.2	20.6	4.2	13.4	+9.2
OpenCLIP ViT-B/32	5.1	13.0	18.5	6.2	14.1	19.8	5.5	12.8	+7.3
OpenAI CLIP ViT-B/32	4.8	12.5	17.7	5.5	13.0	18.5	4.3	12.0	+7.7
RemoteCLIP ViT-B/32	1.1	4.0	6.5	1.5	4.7	7.8	0.8	4.3	+3.5

fixed one-epoch schedule. All fine-tuning and evaluation are restricted to a single GPU by setting `CUDA_VISIBLE_DEVICES=0`, and each configuration is trained once; we therefore report single-run results, plus a three-seed stability check for OpenAI CLIP ViT-B/32 in Sec. 5.2.

5 Experiments

5.1 Evaluation Protocol

The formal CLIP evaluation uses the filtered infrared test split with 9,720 samples after auditing the original 10,000-image test split, and all reported evaluation samples are excluded from fine-tuning. VLM diagnostics use held-out infrared prompts and report task-level averages over the six final VLM backbones; the prompt sampling files are part of the release artifacts. We separate the evaluation by model family because each measures a different aspect of infrared vision-language learning: retrieval evaluates whether infrared images and IR-aware captions are aligned in a shared embedding space, whereas VLM diagnostics evaluate whether an instruction-tuned model produces language grounded in infrared evidence. Combining these into a single aggregate would obscure family-specific failure modes.

5.2 IR-CLIP Retrieval

For IR-CLIP fine-tuning, the image encoder maps the infrared input into a visual embedding, the text encoder maps the IR-aware caption into a language embedding, and a symmetric contrastive objective aligns matched pairs while separating in-batch negatives. This adapts pretrained vision-language priors to infrared remote sensing without relying on RGB appearance, where the visual evidence is dominated by grayscale layout, thermal contrast, sensor-specific texture, fine structural boundaries, and object-background separation. We evaluate five CLIP backbones spanning general and remote-sensing variants to test whether infrared adaptation benefits both generic and geospatially pretrained representations. During fine-tuning, the text side is frozen and the visual tower plus projection layers are adapted, so the main optimization pressure falls on

Table 7: Per-source clean retrieval on the filtered infrared test split, retrieving within each source’s own candidate pool. mR averages R@1, R@5, and R@10 over both directions. Small pools (RSICD, RSITMD) inflate recall and are not directly comparable across sources; sample counts are reported for context.

Source	# Samples	OpenAI ViT-L/14 mR	GeoRSCLIP ViT-B/32 mR
RS5M	7,858	22.8	15.8
SkyScript	1,096	10.8	10.8
NWPU	515	34.0	31.7
RSICD	164	37.7	32.6
RSITMD	87	54.6	54.6

aligning infrared evidence to the existing language space while preserving stable text semantics. This design avoids re-learning the caption space and instead asks the visual encoder to reinterpret infrared patterns as language-grounded remote-sensing concepts. Checkpoints are selected by validation mean recall and used for bidirectional IR-text retrieval.

Table 6 reports clean bidirectional retrieval on the formal filtered test split. OpenAI CLIP ViT-L/14 achieves the strongest result, reaching 19.2% mean recall and leading both retrieval directions across all recall cutoffs. GeoRSCLIP and OpenCLIP form the next tier, while OpenAI CLIP ViT-B/32 remains competitive despite lacking remote-sensing-specific pretraining. RemoteCLIP performs poorly under this infrared split despite remote-sensing adaptation, suggesting that RGB-oriented remote-sensing pretraining does not transfer uniformly when evidence is dominated by grayscale layout, thermal contrast, and sensor-specific texture.

The task remains challenging: even the best model reaches only 8.3% I2T R@1 and 9.5% T2I R@1, since many remote-sensing categories share similar infrared layouts and removing color eliminates shortcuts used by RGB-trained models. The consistent gain of ViT-L/14 over B/32 variants suggests stronger visual capacity helps capture infrared structure under IR-relevant supervision. To calibrate these numbers, the last three columns of Table 6 compare each backbone against its own zero-shot performance using the original pretrained weights without IR-aware fine-tuning. Zero-shot mean recall is low across all backbones (0.8–6.3%), confirming that off-the-shelf CLIP transfers poorly to synthetic infrared imagery, and IR-aware adaptation yields a consistent absolute gain of +3.5 to +12.8 points. This gap shows that the reported scores reflect genuine infrared adaptation rather than residual visible-domain priors, and that MonoIR-RS is non-trivial: infrared alignment must be learned directly rather than inherited from RGB pretraining. To check one representative training run for seed sensitivity, we re-ran OpenAI CLIP ViT-B/32 fine-tuning under three random seeds with an otherwise identical recipe, obtaining a mean recall of 11.9 ± 0.02 (mean \pm standard deviation over seeds). This check indicates low variance for that backbone, while the remaining backbone results are single-run measurements.

Table 7 decomposes the best two backbones by source, retrieving within each source’s own candidate pool. Difficulty varies sharply: SkyScript is hardest (mR \approx 10.8), consistent with its noisy OpenStreetMap-derived supervision;

Table 8: CLIP supervision ablation on a smaller development retrieval split, averaged over five backbones. Original mR and IR-aware mR average R@1, R@5, and R@10 in both retrieval directions; these values are used for recipe comparison and are not directly comparable to the formal 9,720-sample test split.

Supervision setting	Original mR	IR-aware mR
Original-caption only	35.1	30.2
IR-aware-caption only	31.2	43.0
Joint RGB-IR diagnostic	37.0	42.9

RSICD and RSITMD show higher mR largely due to small pools (164 and 87 candidates), so per-source counts are reported. The aggregate in Table 6 is dominated by the large, noisy RS5M and SkyScript pools.

Table 8 reports the supervision ablation motivating the final CLIP recipe on a development retrieval split, whose candidate pool is smaller and therefore not directly comparable to the 9,720-sample formal test split in Table 6. Averaged over five backbones, replacing original captions with IR-aware captions improves development IR-aware retrieval mean recall from 30.2% to 43.0%, showing that infrared-grounded text is a better language target for infrared retrieval under the ablation protocol. Original captions remain stronger on original-text retrieval because they preserve visible-domain wording, but that is not our target setting. A joint RGB-IR diagnostic obtains a similar IR-aware score but is not adopted, since our model-facing setting is infrared-modality inference. The ablation thus supports prioritizing IR-text alignment over RGB-IR matching.

5.3 IR-VLM Understanding Results

We deliberately use *lexical proxy* diagnostics rather than a single accuracy score, because the corpus has no human-verified scene or object labels and the reference captions are machine-generated. Each metric is a keyword-match rate over the generated text, interpreted as a behavior signal, not semantic correctness: **IR-cue rate** is the fraction of answers with an infrared term (e.g. *infrared, thermal, grayscale, intensity, contrast, texture*); **RGB-color rate** (lower better) the fraction with a visible-color word (e.g. *green, blue, red, colorful*); **overclaim rate** (lower better) the fraction asserting unsupported physical detail (e.g. *temperature, heat source, hot, cold*); **class-hit rate** the fraction containing a source-class token; and **average words** the response length. Thus a high IR-cue rate indicates infrared-style phrasing rather than verified grounding, and a low RGB-color rate indicates reduced leakage rather than stronger recognition. The ablations follow the actual development path: IR-aware text supervision for CLIP, and caption-only, class-aware, and multitask instruction data for VLMs.

Table 9 summarizes the clean diagnostic evaluation for the final IR-VLM recipe. Rather than a single accuracy score, each task is checked with script-level diagnostics reflecting the infrared instruction goal: IR-cue mentions, color leakage, overclaim, class-hit, and response length. The table reports averages over the six final backbones for each task type.

Table 9: Clean IR-VLM diagnostic evaluation on held-out infrared prompts, averaged over the six final VLM backbones. IR-cue rate, RGB-color rate, overclaim rate, and class-hit rate are percentages; average words measures response length.

Task	IR-cue rate \uparrow	RGB-color rate \downarrow	Overclaim rate \downarrow	Class-hit rate \uparrow	Avg. words
Infrared image captioning	100.0	0.0	0.07	0.93	17.80
Scene question	64.63	0.0	0.07	0.40	8.05
Object-presence question	0.17	0.0	0.00	0.63	3.40
Infrared-cue explanation	82.73	1.53	10.67	0.60	21.62
Visual-evidence QA	63.63	0.07	19.87	0.83	22.20

The diagnostic results show that the captioning prompt reliably elicits infrared-aware language (100.0% IR-cue rate, almost no overclaiming). Infrared-cue explanation and visual-evidence QA also reference grayscale or thermal evidence frequently, but their higher overclaim rates show that longer explanatory answers introduce unsupported detail. Object-presence prompts are intentionally short, hence low IR-cue rate but nonzero class-hit. Class-hit stays near 1% by design, as it measures literal repetition of the source class token (rare in infrared scene descriptions) and thus acts as a conservative lower-bound signal, not a recognition score. These patterns justify task-separated diagnostics: low RGB-color leakage alone does not imply strong grounding, and high infrared-cue frequency does not guarantee semantic precision.

These patterns also differ across backbones under identical data and prompts. Some models produce longer, more explicitly infrared-aware answers, but this often comes with higher overclaiming because explanatory responses encourage unsupported thermal or physical detail. Others stay short and conservative, reducing hallucinated evidence but also offering weaker infrared-cue coverage. This backbone-dependent trade-off means no single model dominates every diagnostic, and it motivates reporting behavior-specific metrics rather than collapsing VLM performance into one aggregate score.

To confirm that the captioning behavior comes from IR-aware instruction tuning rather than the base models alone, Table 11 compares zero-shot and fine-tuned captioning under the same prompts. The effect is large and consistent for captioning: fine-tuning raises the IR-cue rate to 100% for every backbone (from as low as 4.0% for LLaVA-1.5 and 16.2% for H2RSVLM), eliminates visible-color leakage (e.g. H2RSVLM 16.0% \rightarrow 0.0%, InstructBLIP 3.8% \rightarrow 0.0%), and suppresses overclaiming (Qwen2.5-VL 28.8% \rightarrow 0.4%). The gains are especially meaningful for models whose zero-shot responses either ignore infrared modality cues or revert to generic remote-sensing descriptions. This shows that IR-aware supervision, not the pretrained prior alone, is responsible for infrared-grounded captioning style, reduced color leakage, and more controlled use of thermal evidence.

5.4 VLM Training-Stage Ablation

The VLM training pipeline was developed in several stages, summarized in Table 10. V1 used 5,000 caption-only samples, which were sufficient for teaching

Table 10: VLM training-stage ablation. Development metrics are averaged across the available backbones on a 12-case sanity set; they are used to select the training recipe, while Table 9 reports the formal clean-task evaluation.

Stage	Data size	Main change	IR-cue rate	RGB-word rate	Dev class-hit
Caption-only V1	5,000	Single infrared caption prompt	98.6	0.0	–
Full class-aware V2	48,616	Full train split with scene hints	83.3	0.0	0.0
API-v3 multitask	32,000	30K text QA + 2K vision-audited QA	100.0	0.0	5.6

basic infrared description but too narrow for class-aware or evidence-seeking questions; the model learned to mention infrared cues, yet had little exposure to short discriminative answers or grounded reasoning prompts. V2 expanded to the full train split with class-aware scene hints, improving data coverage but weakening diagnostic balance because the supervision still lacked diverse instruction forms. The selected API-v3 multitask version combines 30,000 text-rewritten QA examples with 2,000 vision-audited examples in a conversation format, training all six backbones after removing malformed rows. This recipe preserves clean infrared-cue behavior while adding explicit scene, object, and evidence instruction types. It therefore gives the best balance of infrared-cue coverage, zero RGB-word leakage, and nonzero class-hit on the sanity set, while better matching the final evaluation tasks in Table 9.

5.5 Dataset Quality Checks

The release-facing checks verify that the benchmark follows the intended split boundary: train–validation, train–test, and validation–test overlaps are all zero, and the referenced infrared paths have no missing-image cases. These checks are essential because MonoIR-RS draws from multiple collections with different naming rules, split conventions, and file organizations, where duplicate, stale, or mixed entries could silently inflate retrieval and instruction-tuning results. The RGB-leakage audit found 280 RGB-named paths in the original 10,000-image test split, which are excluded from the formal evaluation to leave the 9,720-image filtered split used in Table 6. To support reproducibility, error tracing, and independent auditing, the release package includes infrared images, IR-aware captions, split files, filtering logs, and evaluation scripts under a research-use setting; the source imagery inherits the licenses of its original collections. As the data derive from public remote-sensing collections and contain no personally identifiable information, we foresee no direct ethical concerns beyond the synthetic-infrared caveats, possible domain bias, and modality-transfer limitations noted above.

6 Conclusion

This paper presents MonoIR-RS, a large-scale infrared remote-sensing vision-language dataset and benchmark connecting dataset construction, CLIP adaptation, VLM instruction tuning, and data-integrity evaluation under one infrared

Table 11: Zero-shot (original pretrained weights) vs. fine-tuned captioning diagnostics, showing the effect of IR-aware instruction tuning. Values are percentages.

Backbone	IR-cue (zero→ft)	RGB-color (zero→ft)	Overclaim (zero→ft)	Avg. words (zero→ft)
Qwen2.5-VL-7B	98.6 → 100.0	3.4 → 0.0	28.8 → 0.4	24.2 → 17.9
InstructBLIP-FLAN-T5-XL	93.0 → 100.0	3.8 → 0.0	0.0 → 0.0	56.9 → 17.1
LLaVA-1.5-7B	4.0 → 100.0	0.8 → 0.0	0.0 → 0.0	14.2 → 17.8
LLaVA-1.6-Vicuna-7B	72.4 → 100.0	0.0 → 0.0	0.0 → 0.0	11.1 → 18.4
GeoChat-7B	26.8 → 100.0	0.4 → 0.0	0.0 → 0.0	13.8 → 17.9
H2RSVLM-VHM-7B	16.2 → 100.0	16.0 → 0.0	0.0 → 0.0	14.8 → 17.7

protocol. Beyond a set of infrared images, its contribution is an end-to-end workflow that rewrites visible-centric supervision into IR-aware text, enforces train-only hygiene, and evaluates models against zero-shot behavior where available. IR-aware text is essential: development retrieval mean recall rises from 30.2% to 43.0% over original captions under the ablation protocol, the strongest CLIP reaches 19.2% (+12.8 over zero-shot) on the formal filtered test split, and fine-tuning drives VLM captioning IR-cue coverage to 100% while reducing color leakage.

Two limitations bound the scope: the infrared modality is synthesized with DiffV2IR (closer to real infrared than grayscale, but not a sensor substitute), and IR-aware supervision is generated by Qwen2.5-VL-72B, so our diagnostics are lexical proxies rather than human-verified correctness. Future work can extend to real sensor data, more infrared bands, human-verified instructions, and full multi-seed evaluation.

References

1. Astruc, G., Gonthier, N., Mallet, C., Landrieu, L.: Anysat: One earth observation model for many resolutions, scales, and modalities. In: *Proceedings of the Computer Vision and Pattern Recognition Conference*. pp. 19530–19540 (2025)
2. Bai, S., Chen, K., Liu, X., Wang, J., Ge, W., Song, S., Dang, K., Wang, P., Wang, S., Tang, J., Zhong, H., Zhu, Y., Yang, M., Wan, J., Ding, W., Fu, Z., Xu, Y., Ye, J., Zhang, X., Xie, T., Cheng, Z., Zhang, H., Yang, Z., Xu, H., Lin, J.: Qwen2.5-vl technical report (2025)
3. Bi, J., Wang, Y., Chen, H., Xiao, X., Hecker, A., Tresp, V., Ma, Y.: Llava steering: Visual instruction tuning with 500x fewer parameters through modality linear representation-steering. In: *Proceedings of the 63rd Annual Meeting of the Association for Computational Linguistics (Volume 1: Long Papers)*. pp. 15230–15250 (2025)
4. Cao, J., Liu, X., Xue, R.: Firemm-ir: An infrared-enhanced multi-modal large language model for comprehensive scene understanding in remote sensing forest fire monitoring. *Sensors* **26**(2), 390 (2026)
5. Cao, Q., Xu, Z., Chen, Y., Ma, C., Yang, X.: Domain prompt learning with quaternion networks. In: *Proceedings of the IEEE/CVF Conference on Computer Vision and Pattern Recognition*. pp. 26637–26646 (2024)
6. Cao, Z., Zhang, J., Zhang, R.: Irgpt: Understanding real-world infrared image with bi-cross-modal curriculum on large-scale benchmark. In: *Proceedings of the IEEE/CVF International Conference on Computer Vision*. pp. 166–176 (2025)
7. Chen, W., Chen, J., Deng, Y., Chen, J., Feng, Y., Xi, Z., Liu, D., Li, K., Meng, Y.: Lrsclip: A vision-language foundation model for aligning remote sensing image with longer text. In: *Proceedings of the IEEE/CVF Conference on Computer Vision and Pattern Recognition* (2025)
8. Cheng, G., Han, J., Lu, X.: Remote sensing image scene classification: Benchmark and state of the art. *Proceedings of the IEEE* **105**(10), 1865–1883 (2017)
9. Danish, M., Munir, M.A., Shah, S.R.A., Kuckreja, K., Khan, F.S., Fraccaro, P., Lacoste, A., Khan, S.: Geobench-vlm: Benchmarking vision-language models for geospatial tasks. In: *Proceedings of the IEEE/CVF International Conference on Computer Vision*. pp. 7132–7142 (2025)
10. Guo, X., Lao, J., Dang, B., Zhang, Y., Yu, L., Ru, L., Zhong, L., Huang, Z., Wu, K., Hu, D., et al.: Skysense: A multi-modal remote sensing foundation model towards universal interpretation for earth observation imagery. In: *Proceedings of the IEEE/CVF Conference on Computer Vision and Pattern Recognition*. pp. 27672–27683 (2024)
11. Ha, Q., Watanabe, K., Karasawa, T., Ushiku, Y., Harada, T.: Mfnet: Towards real-time semantic segmentation for autonomous vehicles with multi-spectral scenes. In: *2017 IEEE/RSJ International Conference on Intelligent Robots and Systems*. pp. 5108–5115. IEEE (2017)
12. Han, J., Zhang, B., Sun, X., Zhang, Q., Dong, Y., Hu, C., Zhang, F., Wei, Y., Guo, J.: Fusionrs: A large-scale rgb-infrared remote sensing dataset for dual-modal vision-language foundation models. arXiv preprint arXiv:2606.17020 (2026)
13. Han, Z., Zhang, Z., Zhang, S., Zhang, G., Mei, S.: Aerial visible-to-infrared image translation: Dataset, evaluation, and baseline. *Journal of Remote Sensing* **3**, 0096 (2023)
14. Jia, X., Zhu, C., Li, M., Tang, W., Zhou, W.: Llvip: A visible-infrared paired dataset for low-light vision. In: *Proceedings of the IEEE/CVF International Conference on Computer Vision Workshops (ICCVW)*. pp. 3496–3504 (2021)

15. Jiang, S., Chen, Z., Liang, J., Zhao, Y., Liu, M., Qin, B.: Infrared-llava: Enhancing understanding of infrared images in multi-modal large language models. In: Findings of the Association for Computational Linguistics: EMNLP 2024. pp. 8573–8591 (2024)
16. Kuckreja, K., Danish, M.S., Naseer, M., Das, A., Khan, S., Khan, F.S.: Geochat: Grounded large vision-language model for remote sensing. In: Proceedings of the IEEE/CVF conference on computer vision and pattern recognition. pp. 27831–27840 (2024)
17. Li, X., Hong, D., Chanussot, J.: S2mae: A spatial-spectral pretraining foundation model for spectral remote sensing data. In: Proceedings of the IEEE/CVF Conference on Computer Vision and Pattern Recognition. pp. 24088–24097 (2024)
18. Liu, F., Chen, D., Guan, Z., Zhou, X., Zhu, J., Ye, Q., Fu, L., Zhou, J.: Remoteclip: A vision language foundation model for remote sensing. *IEEE Transactions on Geoscience and Remote Sensing* **62**, 1–16 (2024)
19. Liu, H., Li, C., Li, Y., Lee, Y.J.: Improved baselines with visual instruction tuning. In: Proceedings of the IEEE/CVF conference on computer vision and pattern recognition. pp. 26296–26306 (2024)
20. Liu, J., Fan, X., Huang, Z., Wu, G., Liu, R., Zhong, W., Luo, Z.: Target-aware dual adversarial learning and a multi-scenario multi-modality benchmark to fuse infrared and visible for object detection. In: Proceedings of the IEEE/CVF Conference on Computer Vision and Pattern Recognition. pp. 5802–5811 (2022)
21. Lu, X., Wang, B., Zheng, X., Li, X.: Exploring models and data for remote sensing image caption generation. *IEEE Transactions on Geoscience and Remote Sensing* **56**(4), 2183–2195 (2017)
22. Luo, J., Zhang, Y., Yang, X., Wu, K., Zhu, Q., Liang, L., Chen, J., Li, Y.: When large vision-language model meets large remote sensing imagery: Coarse-to-fine text-guided token pruning. In: Proceedings of the IEEE/CVF International Conference on Computer Vision. pp. 9206–9217 (2025)
23. Mall, U.K., Phoo, C.P., Liu, M., Vondrick, C., Hariharan, B., Bala, K.: Remote sensing vision-language foundation models without annotations via ground remote alignment. In: International Conference on Learning Representations. vol. 2024, pp. 49294–49314 (2024)
24. Pang, C., Weng, X., Wu, J., Li, J., Liu, Y., Sun, J., Li, W., Wang, S., Feng, L., Xia, G.S., He, C.: Vhm: Versatile and honest vision language model for remote sensing image analysis. In: Proceedings of the AAAI Conference on Artificial Intelligence. vol. 39, pp. 6381–6388 (2025)
25. Ran, L., Wang, L., Wang, G., Wang, P., Zhang, Y.: Diffv2ir: Visible-to-infrared diffusion model via vision-language understanding. *arXiv preprint arXiv:2503.19012* (2025)
26. Razakarivony, S., Jurie, F.: Vehicle detection in aerial imagery: A small target detection benchmark. *Journal of Visual Communication and Image Representation* **34**, 187–203 (2016)
27. Safaei, B., Siddiqui, F., Xu, J., Patel, V.M., Lo, S.Y.: Filter images first, generate instructions later: Pre-instruction data selection for visual instruction tuning. In: Proceedings of the IEEE/CVF Conference on Computer Vision and Pattern Recognition. pp. 14247–14256 (2025)
28. Soni, S., Dudhane, A., Debary, H., Fiaz, M., Munir, M.A., Danish, M.S., Fraccaro, P., Watson, C.D., Klein, L.J., Khan, F.S., et al.: Earthdial: Turning multi-sensory earth observations to interactive dialogues. In: Proceedings of the Computer Vision and Pattern Recognition Conference. pp. 14303–14313 (2025)

29. Sun, Y., Cao, B., Zhu, P., Hu, Q.: Drone-based rgb-infrared cross-modality vehicle detection via uncertainty-aware learning. *IEEE Transactions on Circuits and Systems for Video Technology* **32**(10), 6700–6713 (2022)
30. Wang, Z., Prabha, R., Huang, T., Wu, J., Rajagopal, R.: Skyscript: A large and semantically diverse vision-language dataset for remote sensing. In: *Proceedings of the AAAI Conference on Artificial Intelligence*. vol. 38, pp. 5805–5813 (2024)
31. Wen, X., Zhao, B., Chen, Y., Pang, J., Qi, X.: What makes clip more robust to long-tailed pre-training data? a controlled study for transferable insights. *Advances in Neural Information Processing Systems* **37**, 36567–36601 (2024)
32. Yuan, Z., Zhang, W., Fu, K., Li, X., Deng, C., Wang, H., Sun, X.: Exploring a fine-grained multiscale method for cross-modal remote sensing image retrieval. *IEEE Transactions on Geoscience and Remote Sensing* **60**, 1–19 (2021)
33. Zanella, M., Gérin, B., Ayed, I.B.: Boosting vision-language models with transduction. *Advances in Neural Information Processing Systems* **37**, 62223–62256 (2024)
34. Zhang, S., Fang, Q., Yang, Y., Feng, Y.: Llava-mini: Efficient image and video large multimodal models with one vision token. In: *International Conference on Learning Representations*. vol. 2025, pp. 53285–53310 (2025)
35. Zhang, Z., Zhao, T., Guo, Y., Yin, J.: Rs5m and georsclip: A large-scale vision-language dataset and a large vision-language model for remote sensing. *IEEE Transactions on Geoscience and Remote Sensing* **62**, 1–23 (2024)
36. Zhu, Q., Lao, J., Ji, D., Luo, J., Wu, K., Zhang, Y., Ru, L., Wang, J., Chen, J., Yang, M., et al.: Skysense-o: Towards open-world remote sensing interpretation with vision-centric visual-language modeling. In: *Proceedings of the IEEE/CVF Conference on Computer Vision and Pattern Recognition*. pp. 14733–14744 (2025)

A Mathematical Formulation and Algorithms

This appendix formalizes the dataset construction, model adaptation, and evaluation metrics used in the main paper. The notation follows the implementation used for the reported IR-CLIP and IR-VLM experiments: CLIP models are fine-tuned with a symmetric image-text contrastive loss, VLMs are adapted with instruction-following loss and LoRA adapters, and VLM behavior is evaluated with lexical diagnostics rather than human-verified semantic accuracy.

A.1 Notation

Let the source remote-sensing pool be

$$\mathcal{S} = \{(I_i^{\text{rgb}}, c_i, s_i, d_i)\}_{i=1}^N, \quad N = 600,000, \quad (1)$$

where I_i^{rgb} is the visible-band source image, c_i is the original source caption or metadata text, $s_i \in \{\text{train}, \text{val}, \text{test}\}$ is the split, and d_i is the source dataset identifier. The model-facing infrared image is generated by a visible-to-infrared translation function,

$$I_i^{\text{ir}} = T_\phi(I_i^{\text{rgb}}), \quad (2)$$

where T_ϕ denotes the DiffV2IR-based synthesis pipeline used in the paper. The IR-aware text is written as

$$t_i = R_\omega(I_i^{\text{rgb}}, I_i^{\text{ir}}, c_i), \quad (3)$$

where R_ω denotes the IR-aware caption rewriting process. The RGB image is used only at construction time to preserve scene semantics during rewriting; the model-facing example used for fine-tuning and evaluation is

$$x_i = (I_i^{\text{ir}}, t_i, s_i, d_i). \quad (4)$$

For CLIP-style fine-tuning, each retained training item is an image-text pair (I_i^{ir}, t_i) . For VLM instruction tuning, a train-only subset of retained records is converted into an instruction triple

$$z_i = (I_i^{\text{ir}}, q_i, a_i), \quad (5)$$

where q_i is a task prompt and a_i is the target answer. The final API-v3 multitask VLM recipe uses 32,000 train-split conversations constructed from the retained training pool.

A.2 Filtering and Split Hygiene

The retained IR-aware caption set is defined by a binary validity predicate

$$m_i = \mathbf{1} [I_i^{\text{ir}} \text{ exists} \wedge |t_i| > 0 \wedge s_i \in \{\text{train}, \text{val}, \text{test}\} \wedge Q(x_i) = \text{pass}], \quad (6)$$

where $Q(\cdot)$ summarizes the quality checks for empty entries, malformed split fields, missing images, weak IR descriptions, and unsupported text. The retained split-specific sets are

$$\mathcal{D}_s = \{x_i : m_i = 1, s_i = s\}, \quad s \in \{\text{train, val, test}\}. \quad (7)$$

The paper uses $|\mathcal{D}_{\text{train}}| = 48,616$, $|\mathcal{D}_{\text{val}}| = 416$, and $|\mathcal{D}_{\text{test}}| = 10,000$ IR-aware caption records. CLIP uses the retained train records as image-text pairs. The final VLM recipe uses $\mathcal{Z}_{\text{train}} \subset \mathcal{D}_{\text{train}}$, with $|\mathcal{Z}_{\text{train}}| = 32,000$ conversations.

For the formal CLIP retrieval evaluation, we further apply a path-level audit and remove test entries whose path strings indicate residual visible-band naming. Let

$$\rho_i = \mathbf{1}[\text{"rgb"} \in \text{lowercase}(\text{path}(I_i^{\text{ir}}))]. \quad (8)$$

The filtered evaluation set is

$$\mathcal{D}_{\text{test}}^{\text{clean}} = \{x_i \in \mathcal{D}_{\text{test}} : \rho_i = 0\}, \quad |\mathcal{D}_{\text{test}}^{\text{clean}}| = 9,720. \quad (9)$$

This audit is deliberately conservative and file-name based: it prevents path-level visible-band leakage in the reported retrieval surface, but it is not a content-level detector of all possible source-domain artifacts. The release keeps the flagged list so that stronger content-level audits can be added without changing the reported split definition. Equivalently, the model-facing sets used by the two training stages are

$$\mathcal{P}_{\text{CLIP}} = \{(I_i^{\text{ir}}, t_i) : x_i \in \mathcal{D}_{\text{train}}\}, \quad (10)$$

$$\mathcal{Z}_{\text{train}} = \{G_\xi(x_i) : x_i \in \mathcal{D}_{\text{train}}, h_\xi(x_i) = 1\}, \quad |\mathcal{Z}_{\text{train}}| = 32,000, \quad (11)$$

$$\mathcal{E}_{\text{CLIP}} = \mathcal{D}_{\text{test}}^{\text{clean}}, \quad (12)$$

where G_ξ converts a retained train record into an instruction tuple and h_ξ denotes the API-v3 multitask selection and validity filter.

A.3 Synthetic-IR Realism Metrics

To compare synthetic infrared images with real infrared images from AVIID, the main paper reports FID and grayscale-histogram distances. Let \mathcal{X} and \mathcal{Y} be two image sets, and let $\mu_{\mathcal{X}}, \Sigma_{\mathcal{X}}$ and $\mu_{\mathcal{Y}}, \Sigma_{\mathcal{Y}}$ be the mean and covariance of their Inception features. The Fréchet Inception Distance is

$$\text{FID}(\mathcal{X}, \mathcal{Y}) = \|\mu_{\mathcal{X}} - \mu_{\mathcal{Y}}\|_2^2 + \text{Tr} \left(\Sigma_{\mathcal{X}} + \Sigma_{\mathcal{Y}} - 2(\Sigma_{\mathcal{X}}\Sigma_{\mathcal{Y}})^{1/2} \right). \quad (13)$$

For grayscale histograms, let $p, q \in \mathbb{R}^B$ be normalized intensity histograms with $\sum_{b=1}^B p_b = \sum_{b=1}^B q_b = 1$. With a small numerical constant $\epsilon > 0$, the

histogram metrics are

$$D_{\text{KL}}(p\|q) = \sum_{b=1}^B p_b \log \frac{p_b + \epsilon}{q_b + \epsilon}, \quad (14)$$

$$D_{\text{JS}}(p, q) = \frac{1}{2} D_{\text{KL}}(p\|m) + \frac{1}{2} D_{\text{KL}}(q\|m), \quad m = \frac{p+q}{2}, \quad (15)$$

$$\chi^2(p, q) = \frac{1}{2} \sum_{b=1}^B \frac{(p_b - q_b)^2}{p_b + q_b + \epsilon}, \quad (16)$$

$$\text{HI}(p, q) = \sum_{b=1}^B \min(p_b, q_b). \quad (17)$$

Lower values are better for FID, KL, JS, and χ^2 , while higher values are better for histogram intersection.

A.4 IR-CLIP Contrastive Objective

For a mini-batch of B retained image-text pairs $\{(I_i^{\text{ir}}, t_i)\}_{i=1}^B$, the image encoder f_θ and text encoder g_ψ produce normalized embeddings

$$u_i = \frac{f_\theta(I_i^{\text{ir}})}{\|f_\theta(I_i^{\text{ir}})\|_2}, \quad v_i = \frac{g_\psi(t_i)}{\|g_\psi(t_i)\|_2}. \quad (18)$$

The implementation freezes the text side when `freeze-text` is enabled and updates the visual tower, projection parameters, and logit scale. Let $\alpha = \exp(\gamma)$ be the learned logit scale. The image-text similarity logits are

$$z_{ij} = \alpha u_i^\top v_j. \quad (19)$$

The image-to-text and text-to-image losses are

$$\mathcal{L}_{I \rightarrow T} = -\frac{1}{B} \sum_{i=1}^B \log \frac{\exp(z_{ii})}{\sum_{j=1}^B \exp(z_{ij})}, \quad (20)$$

$$\mathcal{L}_{T \rightarrow I} = -\frac{1}{B} \sum_{i=1}^B \log \frac{\exp(z_{ii})}{\sum_{j=1}^B \exp(z_{ji})}. \quad (21)$$

The final symmetric contrastive loss is

$$\mathcal{L}_{\text{CLIP}} = \frac{1}{2} (\mathcal{L}_{I \rightarrow T} + \mathcal{L}_{T \rightarrow I}). \quad (22)$$

A.5 Retrieval Metrics

For a retrieval set of M paired examples, let U and V denote the normalized image and text embeddings. The correct text for image i is v_i , and the correct

image for text i is u_i . The rank of the paired text under image-to-text retrieval is

$$r_i^{I \rightarrow T} = 1 + \sum_{j \neq i} \mathbf{1}[u_i^\top v_j > u_i^\top v_i]. \quad (23)$$

The rank $r_i^{T \rightarrow I}$ is defined analogously by ranking images for text query v_i . Recall at K is

$$R_{I \rightarrow T} @ K = \frac{1}{M} \sum_{i=1}^M \mathbf{1}[r_i^{I \rightarrow T} \leq K], \quad (24)$$

with $R_{T \rightarrow I} @ K$ defined similarly. The mean recall reported in the paper averages the three recall cutoffs in both retrieval directions:

$$\text{mR} = \frac{1}{6} \sum_{K \in \{1, 5, 10\}} (R_{I \rightarrow T} @ K + R_{T \rightarrow I} @ K). \quad (25)$$

The same definition is used for the synthetic-IR retrieval benchmark and the AVIID paired retrieval sanity check, with only the query and gallery modalities changed. Checkpoint selection is written as

$$c^* = \arg \max_{c \in \mathcal{C}} \text{mR}_{\text{val}}(c), \quad (26)$$

$$\text{Score}_{\text{test}} = \{R_{I \rightarrow T} @ K, R_{T \rightarrow I} @ K\}_{K \in \{1, 5, 10\}} \Big|_{\mathcal{D}_{\text{test}}^{\text{clean}, c^*}}. \quad (27)$$

A.6 IR-VLM Instruction-Tuning Objective

For VLM training, each example is represented as $(I_i^{\text{ir}}, q_i, a_i) \in \mathcal{Z}_{\text{train}}$, where q_i is the instruction and $a_i = (a_{i,1}, \dots, a_{i,L_i})$ is the target answer. The visual encoder E_η produces visual tokens, and a multimodal projector P_ω maps them into the language-model embedding space when the backbone exposes such a projector:

$$H_i = P_\omega(E_\eta(I_i^{\text{ir}})). \quad (28)$$

The instruction-tuned language model predicts answer tokens conditioned on the visual tokens and the user prompt:

$$p_\Theta(a_i | I_i^{\text{ir}}, q_i) = \prod_{\ell=1}^{L_i} p_\Theta(a_{i,\ell} | H_i, q_i, a_{i,<\ell}). \quad (29)$$

Only assistant-answer tokens contribute to the supervised loss; prompt tokens are masked. The training objective is

$$\mathcal{L}_{\text{VLM}} = -\frac{1}{\sum_i L_i} \sum_i \sum_{\ell=1}^{L_i} \log p_\Theta(a_{i,\ell} | H_i, q_i, a_{i,<\ell}). \quad (30)$$

The selected adapter parameters are therefore

$$\Theta^* = \arg \min_{\Theta_{\text{LoRA}}, \omega} \mathcal{L}_{\text{VLM}}(\mathcal{Z}_{\text{train}}; \Theta, \omega), \quad (31)$$

with the base language model parameters fixed.

Parameter-efficient adaptation is implemented with LoRA. For a frozen linear layer $W \in \mathbb{R}^{d_{\text{out}} \times d_{\text{in}}}$, LoRA replaces the effective weight by

$$W' = W + \Delta W, \quad \Delta W = \frac{\alpha_{\text{LoRA}}}{r} BA, \quad (32)$$

where $A \in \mathbb{R}^{r \times d_{\text{in}}}$ and $B \in \mathbb{R}^{d_{\text{out}} \times r}$ are trainable low-rank matrices. The experiments use $r = 32$, $\alpha_{\text{LoRA}} = 64$, and dropout 0.05. For Qwen2.5-VL, LoRA is applied to attention and MLP projection modules. For InstructBLIP, LoRA is applied to the query and value modules. For LLaVA-style, GeoChat, and H2RSVLM-style models, LoRA adapters and the exposed multimodal projector are trained while the base LLM is kept fixed.

A.7 VLM Diagnostic Metrics

The VLM metrics in the main paper are lexical diagnostics, not human-verified semantic accuracy. For n generated answers $\{y_i\}_{i=1}^n$, define keyword sets \mathcal{K}_{IR} , \mathcal{K}_{RGB} , and $\mathcal{K}_{\text{over}}$ for infrared evidence terms, visible-color terms, and unsupported thermal overclaim terms. Let $\text{hit}(y, \mathcal{K})$ be one when any keyword in \mathcal{K} appears in y , and zero otherwise. Then

$$\text{IRCueRate} = \frac{100}{n} \sum_{i=1}^n \text{hit}(y_i, \mathcal{K}_{\text{IR}}), \quad (33)$$

$$\text{RGBColorRate} = \frac{100}{n} \sum_{i=1}^n \text{hit}(y_i, \mathcal{K}_{\text{RGB}}), \quad (34)$$

$$\text{OverclaimRate} = \frac{100}{n} \sum_{i=1}^n \text{hit}(y_i, \mathcal{K}_{\text{over}}). \quad (35)$$

The class-hit diagnostic uses a source class token set \mathcal{C}_i extracted from the source class name or task metadata:

$$\text{ClassHitRate} = \frac{100}{n} \sum_{i=1}^n \mathbf{1}[\text{tokens}(y_i) \cap \mathcal{C}_i \neq \emptyset]. \quad (36)$$

The average response length is

$$\text{AvgWords} = \frac{1}{n} \sum_{i=1}^n |\text{words}(y_i)|. \quad (37)$$

The reported task-level diagnostic vector is

$$\mathbf{m}_\tau = \begin{bmatrix} \text{IRCueRate}_\tau \\ \text{RGBColorRate}_\tau \\ \text{OverclaimRate}_\tau \\ \text{ClassHitRate}_\tau \\ \text{AvgWords}_\tau \end{bmatrix}, \quad (38)$$

Algorithm 1 Infrared record construction

Require: $\mathcal{S}, T_\phi, R_\omega, Q, h_\xi, G_\xi$
Ensure: $\{\mathcal{D}_s\}_s, \mathcal{P}_{\text{CLIP}}, \mathcal{Z}_{\text{train}}, \mathcal{D}_{\text{test}}^{\text{clean}}$

- 1: **for** $i = 1, \dots, N$ **do**
- 2: **Synthesize and rewrite:** $I_i^{\text{ir}} \leftarrow T_\phi(I_i^{\text{rgb}}), t_i \leftarrow R_\omega(I_i^{\text{rgb}}, I_i^{\text{ir}}, c_i)$
- 3: **Form one candidate record:** $x_i \leftarrow (I_i^{\text{ir}}, t_i, s_i, d_i)$
- 4: **Apply quality gate:** $m_i \leftarrow \mathbf{1}[I_i^{\text{ir}} \text{ exists} \wedge |t_i| > 0$
 $\wedge s_i \in \{\text{train, val, test}\} \wedge Q(x_i) = \text{pass}]$
- 5: **end for**
- 6: **Retain split records:** $\mathcal{D}_s \leftarrow \{x_i : m_i = 1, s_i = s\}, s \in \{\text{train, val, test}\}$
- 7: **Derive CLIP pairs:** $\mathcal{P}_{\text{CLIP}} \leftarrow \{(I_i^{\text{ir}}, t_i) : x_i \in \mathcal{D}_{\text{train}}\}$
- 8: **Derive VLM conversations:** $\mathcal{Z}_{\text{train}} \leftarrow \{G_\xi(x_i) : x_i \in \mathcal{D}_{\text{train}}, h_\xi(x_i) = 1\}$
- 9: **Clean retrieval test:** $\mathcal{D}_{\text{test}}^{\text{clean}} \leftarrow \{x_i \in \mathcal{D}_{\text{test}} : \rho_i = 0\}$

Algorithm 2 IR-CLIP contrastive adaptation and retrieval

Require: $\mathcal{P}_{\text{CLIP}}, \mathcal{D}_{\text{val}}, \mathcal{D}_{\text{test}}^{\text{clean}}$
Ensure: $c^*, \text{Score}_{\text{test}}$

- 1: **Set trainable parameters:** $\Omega_{\text{CLIP}} = \{\theta_{\text{vis}}, \theta_{\text{proj}}, \gamma\}, \psi \leftarrow \psi_0$
- 2: **for** $e = 1, \dots, E$ **do**
- 3: **Optimize contrastive objective:**
 $\Omega_{\text{CLIP}}^{(e)} \leftarrow \arg \min_{\Omega_{\text{CLIP}}} \sum_{(I,t) \in \mathcal{P}_{\text{CLIP}}} \mathcal{L}_{\text{CLIP}}(I, t; \Omega_{\text{CLIP}}, \psi_0)$
- 4: **Save candidate checkpoint:** $c_e \leftarrow \Omega_{\text{CLIP}}^{(e)}$
- 5: **end for**
- 6: **Select by validation retrieval:** $c^* \leftarrow \arg \max_{c \in \{c_e\}_{e=1}^E} \text{mR}_{\text{val}}(c)$
- 7: **Report held-out retrieval:**
 $\text{Score}_{\text{test}} \leftarrow \{R_{I \rightarrow T} @ K, R_{T \rightarrow I} @ K\}_{K \in \{1, 5, 10\}} \Big|_{\mathcal{D}_{\text{test}}^{\text{clean}}, c^*}$

where τ indexes the prompt type. These diagnostics are intentionally conservative. A high IR-cue rate indicates that the response uses infrared-style evidence language, while a low RGB-color rate indicates reduced visible-color leakage. Neither should be interpreted as object-level or scene-level semantic accuracy.

Algorithms 1–3 summarize how the equations above are instantiated in the experimental pipeline. Each algorithm keeps the operational step in text and places the actual transformation or selection rule in mathematical form, so that the appendix remains reproducible without duplicating implementation details from the code.

A.8 Implementation Traceability

The equations above correspond to the experimental scripts used to produce the paper tables. The CLIP objective follows the symmetric cross-entropy implementation used for both HuggingFace CLIP and OpenCLIP backbones. Retrieval metrics follow the evaluation routine that computes top- K hits from the image-text similarity matrix and then averages $R@1$, $R@5$, and $R@10$ across the two directions. The VLM objective follows the train-only multitask QA scripts,

Algorithm 3 IR-VLM instruction adaptation and diagnostics

Require: $\mathcal{Z}_{\text{train}}, \mathcal{H}_\tau, \Theta_0$

Ensure: Θ^* and $\{\mathbf{m}_\tau\}_\tau$

- 1: **Set trainable parameters:** $\Omega_{\text{VLM}} = \{\Theta_{\text{LoRA}}, \omega\}, \Theta_{\text{base}} \leftarrow \Theta_0$
 - 2: **Fit adapters on train-only conversations:**
 $\Omega_{\text{VLM}}^* \leftarrow \arg \min_{\Omega_{\text{VLM}}} \mathcal{L}_{\text{VLM}}(\mathcal{Z}_{\text{train}}; \Omega_{\text{VLM}}, \Theta_0)$
 - 3: **for all** τ **do**
 - 4: **for all** $(I_j^{\text{ir}}, q_j) \in \mathcal{H}_\tau$ **do**
 - 5: **Generate answer:** $y_j \leftarrow \arg \max_y p_{\Omega_{\text{VLM}}^*, \Theta_0}(y | I_j^{\text{ir}}, q_j)$
 - 6: **end for**
 - 7: **Compute lexical diagnostics:** $\mathbf{m}_\tau \leftarrow [\text{IR}_\tau, \text{RGB}_\tau, \text{Over}_\tau, \text{Class}_\tau, \text{Len}_\tau]$
 - 8: **end for**
 - 9: $\Theta^* \leftarrow (\Omega_{\text{VLM}}^*, \Theta_0)$
-

where labels are applied only to assistant answer tokens. The VLM diagnostic metrics follow the clean evaluation scripts that count infrared evidence words, visible-color words, overclaim words, class-token hits, and response length.

B Supplementary Experimental Results

This appendix expands the aggregate tables of the main paper into per-backbone, per-source, and per-configuration form. It is intended to expose the variation that is compressed by averaged results, including backbone-specific retrieval behavior, source-dependent gallery difficulty, auxiliary paired-retrieval transfer, and seed-level stability. All numbers are taken directly from the evaluation outputs used for the main paper; no values are re-estimated or post-processed beyond table formatting.

B.1 Extended Per-Source Retrieval

Table 12 gives the full bidirectional recall behind the per-source summary of the main paper, for the two strongest CLIP backbones, retrieving within each source’s own candidate pool. This breakdown is useful because a single pooled score mixes backbone alignment quality, gallery size, caption noise, and repeated remote-sensing layouts. The source-difficulty ordering is consistent across both backbones: SkyScript is hardest because its OpenStreetMap-derived supervision is noisier and less caption-like, while the small RSICD and RSITMD pools inflate recall by presenting fewer competing candidates. We therefore report their sample counts directly. Per-source retrieval was computed only for these two backbones; for completeness, Table 13 lists the pooled mean recall of all five CLIP backbones on the merged 9,720-image split.

Table 12: Full per-source bidirectional recall (%) for the two strongest CLIP backbones on the filtered infrared test split, retrieving within each source’s candidate pool. I2T is image-to-text, T2I is text-to-image; mR averages all six recall values.

Source	#	I2T R@1	I2T R@5	I2T R@10	T2I R@1	T2I R@5	T2I R@10	mR
OpenAI CLIP ViT-L/14								
RS5M	7,858	10.13	23.61	32.09	11.53	25.49	33.76	22.77
SkyScript	1,096	3.28	9.31	15.51	4.47	12.77	19.43	10.80
NWPU	515	12.23	34.56	49.32	11.84	40.58	55.15	33.95
RSICD	164	15.24	40.85	54.27	13.41	43.29	59.15	37.70
RSITMD	87	17.24	57.47	77.01	28.74	66.67	80.46	54.60
GeoRSCLIP ViT-B/32								
RS5M	7,858	6.58	16.80	24.13	6.62	16.79	24.14	15.84
SkyScript	1,096	3.56	9.31	14.96	4.38	13.23	19.07	10.75
NWPU	515	12.04	32.23	48.74	12.23	34.17	50.68	31.68
RSICD	164	12.20	32.32	48.17	13.41	36.59	53.05	32.62
RSITMD	87	22.99	60.92	74.71	25.29	64.37	79.31	54.60

The per-source table explains why the same checkpoint can look stronger or weaker depending on the gallery being queried. Smaller caption datasets produce higher recall partly because they have fewer competing candidates, while larger sources expose noisier supervision and more visually repeated layouts. This is why the appendix reports both source-specific and pooled retrieval instead of using only the most favorable view.

Table 13: Pooled bidirectional recall (%) of all five CLIP backbones on the merged 9,720-image filtered test split (all sources in one candidate pool). mR averages the six recall values and matches the fine-tuned column of the main-paper retrieval table.

Backbone	I2T R@1	I2T R@5	I2T R@10	T2I R@1	T2I R@5	T2I R@10	mR
OpenAI CLIP ViT-L/14	8.33	19.78	27.14	9.50	21.43	28.80	19.16
GeoRSCLIP ViT-B/32	5.32	14.15	20.43	5.56	14.22	20.57	13.37
OpenCLIP ViT-B/32	5.13	13.01	18.48	6.21	14.15	19.81	12.80
OpenAI CLIP ViT-B/32	4.76	12.46	17.69	5.49	13.05	18.52	11.99
RemoteCLIP ViT-B/32	1.14	3.97	6.50	1.48	4.72	7.82	4.27

The pooled results in Table 13 should be read together with Table 12. Per-source evaluation explains where the model succeeds or struggles, whereas pooled evaluation reflects the harder deployment-like setting in which all sources compete in the same gallery. The gap between RS5M/SkyScript and the smaller caption datasets also warns against over-reading per-source recall without considering candidate-pool size and supervision noise.

B.2 Auxiliary AVIID Paired Retrieval

Table 14 gives the full paired image-image retrieval behind the auxiliary AVIID sanity check summarized in the main paper. Two configurations are evaluated on the 804 AVIID test triplets: configuration A retrieves between real infrared and visible images, and configuration C retrieves between real infrared and DiffV2IR-synthesized infrared. In both configurations the IR-aware fine-tuned CLIP improves over its zero-shot counterpart in every direction and at every cutoff, with mean-recall gains of +6.5 (A) and +23.4 (C) points. Because the fine-tuning never uses AVIID data, this result provides limited auxiliary evidence of cross-dataset transfer under paired retrieval, rather than a claim of full real-sensor generalization.

Table 14: Full AVIID paired image-image retrieval sanity check (%) with OpenAI CLIP ViT-L/14, zero-shot vs. IR-aware fine-tuned, on 804 test triplets. Configuration A: real-IR \leftrightarrow visible; configuration C: real-IR \leftrightarrow synthetic-IR. mR averages the six recall values per configuration.

Config.	Direction	R@1	R@5	R@10	mR
Zero-shot (original pretrained weights)					
A: real-IR \leftrightarrow visible	IR \rightarrow RGB	2.74	12.44	19.78	12.17
	RGB \rightarrow IR	3.73	13.68	20.65	
C: real-IR \leftrightarrow synthetic-IR	IR \rightarrow Syn	7.46	23.51	36.44	19.84
	Syn \rightarrow IR	3.98	18.91	28.73	
IR-aware fine-tuned					
A: real-IR \leftrightarrow visible	IR \rightarrow RGB	4.48	15.42	25.12	18.70
	RGB \rightarrow IR	6.72	24.75	35.70	
C: real-IR \leftrightarrow synthetic-IR	IR \rightarrow Syn	21.02	50.87	62.56	43.24
	Syn \rightarrow IR	18.41	46.89	59.70	

This auxiliary result is included to make the synthetic-to-real boundary explicit. The improvement on AVIID indicates that the selected CLIP checkpoint is not merely memorizing the synthetic benchmark surface, but the experiment is still a small paired-retrieval check rather than a full real-sensor benchmark. We therefore use it as supporting evidence for representation transfer and keep the main claims tied to the controlled MonoIR-RS evaluation.

B.3 Seed Stability

Table 15 expands the seed-stability check of the main paper. OpenAI CLIP ViT-B/32 is fine-tuned under three random seeds with an otherwise identical recipe and evaluated on the 9,720-image filtered split. The mean recall is 11.88 ± 0.02 (sample standard deviation over seeds), suggesting that this backbone is stable under the tested recipe rather than driven by a single-run artifact.

Table 15: Seed-stability check for OpenAI CLIP ViT-B/32 on the 9,720-image filtered split. I2T is IR→IR-aware-text, T2I is the reverse; mR averages the six recall values.

Seed	I2T R@1	I2T R@5	I2T R@10	T2I R@1	T2I R@5	T2I R@10	mR
1	4.73	12.13	17.49	5.28	13.02	18.76	11.90
2	4.69	12.25	17.52	5.35	12.95	18.58	11.89
3	4.56	12.25	17.48	5.35	12.97	18.53	11.86
Mean \pm std							11.88 \pm 0.02

The seed check is deliberately narrow. It controls for run-to-run variation on one representative CLIP backbone and confirms that the reported OpenAI CLIP ViT-B/32 result is not an obvious single-seed outlier. It does not replace a full multi-seed study over every backbone, which remains a larger-scale reproducibility extension.

B.4 Per-Backbone VLM Lexical Diagnostics

Table 16 reports the five lexical diagnostics for all six IR-VLM backbones on every evaluation task (500 held-out prompts per task; all prompts returned parseable text). The aggregate table in the main paper averages each column over these backbones. The per-backbone view exposes the trade-off discussed in the main text: on explanatory prompts (Infrared-cue explanation, Visual-evidence QA) the backbones that reach the highest lexical IR-cue rates, such as Qwen2.5-VL and H2RSVLM, also produce the longest answers and the highest overclaim rates, whereas InstructBLIP stays short and conservative with much lower IR-cue rates. No single backbone dominates all five diagnostics simultaneously, which is why the paper reports behavior-specific lexical metrics rather than one aggregate score.

Table 16: Per-backbone IR-VLM lexical diagnostics across the seven evaluation tasks (500 prompts each). IR-cue, RGB-color, overclaim, and class-hit are percentages; avg. words is response length. RGB-color and overclaim are lower-is-better; IR-cue and class-hit are higher-is-better. These metrics describe response wording and do not measure full semantic correctness.

Task	Backbone	IR-cue \uparrow	RGB-color \downarrow	Overclaim \downarrow	Class-hit \uparrow	Avg. words
Captioning	Qwen2.5-VL-7B	100.0	0.0	0.4	0.8	17.9
	InstructBLIP-FLAN-T5-XL	100.0	0.0	0.0	1.0	17.1
	LLaVA-1.5-7B	100.0	0.0	0.0	1.0	17.8
	LLaVA-1.6-Vicuna-7B	100.0	0.0	0.0	0.8	18.4
	GeoChat-7B	100.0	0.0	0.0	0.8	17.9
	H2RSVLM-VHM-7B	100.0	0.0	0.0	1.2	17.7
Scene question	Qwen2.5-VL-7B	58.8	0.0	0.0	0.4	7.9
	InstructBLIP-FLAN-T5-XL	12.4	0.0	0.0	0.2	2.4
	LLaVA-1.5-7B	82.4	0.0	0.2	0.4	9.9
	LLaVA-1.6-Vicuna-7B	88.2	0.0	0.2	0.2	11.0
	GeoChat-7B	79.6	0.0	0.0	0.6	9.7
	H2RSVLM-VHM-7B	66.4	0.0	0.0	0.6	7.4
Object presence	Qwen2.5-VL-7B	0.4	0.0	0.0	0.8	3.3
	InstructBLIP-FLAN-T5-XL	0.0	0.0	0.0	0.6	3.1
	LLaVA-1.5-7B	0.0	0.0	0.0	0.6	3.5
	LLaVA-1.6-Vicuna-7B	0.0	0.0	0.0	0.4	3.5
	GeoChat-7B	0.4	0.0	0.0	0.4	3.6
	H2RSVLM-VHM-7B	0.2	0.0	0.0	1.0	3.4
Infrared-cue expl.	Qwen2.5-VL-7B	100.0	0.0	9.4	0.8	28.1
	InstructBLIP-FLAN-T5-XL	100.0	0.0	0.0	0.4	12.8
	LLaVA-1.5-7B	60.6	2.6	7.0	0.6	13.7
	LLaVA-1.6-Vicuna-7B	79.2	2.0	12.0	0.2	15.4
	GeoChat-7B	56.6	1.8	10.8	0.4	13.8
	H2RSVLM-VHM-7B	100.0	2.8	24.8	1.2	45.9
Hard scene	Qwen2.5-VL-7B	61.2	0.0	0.0	0.6	12.9
	InstructBLIP-FLAN-T5-XL	0.0	0.0	0.0	0.2	1.2
	LLaVA-1.5-7B	73.8	0.0	0.0	0.2	12.8
	LLaVA-1.6-Vicuna-7B	64.4	0.0	0.0	0.6	14.5
	GeoChat-7B	72.8	0.0	0.0	0.4	14.2
	H2RSVLM-VHM-7B	58.4	0.0	0.0	0.6	13.4
Hard-negative	Qwen2.5-VL-7B	26.6	1.4	0.0	0.4	15.6
	InstructBLIP-FLAN-T5-XL	2.0	0.0	0.0	0.2	1.5
	LLaVA-1.5-7B	65.8	3.2	0.0	1.0	18.1
	LLaVA-1.6-Vicuna-7B	35.4	0.6	0.0	1.0	28.0
	GeoChat-7B	46.6	1.4	0.0	1.6	30.2
	H2RSVLM-VHM-7B	30.8	0.0	0.0	1.0	26.6
Visual-evidence QA	Qwen2.5-VL-7B	100.0	0.0	33.4	1.4	35.1
	InstructBLIP-FLAN-T5-XL	100.0	0.0	16.2	1.2	33.5
	LLaVA-1.5-7B	26.0	0.0	8.8	0.4	10.0
	LLaVA-1.6-Vicuna-7B	28.4	0.0	7.8	0.6	10.1
	GeoChat-7B	27.4	0.2	7.6	0.4	9.6
	H2RSVLM-VHM-7B	100.0	0.2	45.4	1.0	34.9

The per-backbone table is intended as a diagnostic breakdown rather than a leaderboard. It shows that the selected VLM recipe makes captioning consistently use infrared-style language, while explanatory prompts remain more fragile because longer answers increase unsupported physical wording. The practical conclusion is therefore bounded: the fine-tuned VLMs are usable as first-version infrared instruction models, but their open-ended reasoning should still be interpreted through the lexical checks defined in Appendix A.7.

C Reproducibility Details

This appendix reports the prompts, hyperparameters, and generation settings used to produce the dataset and all reported results. Values are transcribed from the release scripts.

C.1 VLM Instruction and Evaluation Prompts

The final API-v3 multitask recipe covers seven prompt types. Each training instruction is prefixed with the image token; the answers are rewritten by a text model and audited by a vision model before use. Table 17 lists the evaluation prompts (500 held-out infrared images per task) verbatim.

Table 17: Evaluation prompts for the seven IR-VLM diagnostic tasks. Each row defines one fixed held-out prompt template used for VLM behavior analysis; the left column names the diagnostic task, and the right column gives the exact prompt issued to each model. The prompt set covers concise captioning, scene classification, object listing, evidence-grounded explanation, visual-evidence QA, hard scene discrimination, and hard-negative contrast under the same infrared remote-sensing image pool.

Task	Prompt
Infrared image captioning	Describe this infrared remote-sensing image in one concise sentence.
Scene classification	Classify the scene type in this infrared remote-sensing image. Answer with the scene name and one short visual reason.
Object presence	List the main visible objects or land-cover elements in this infrared remote-sensing image.
Infrared-cue explanation	Explain the infrared visual cues that support your interpretation of this image.
Visual-evidence QA	What visible infrared evidence supports the scene interpretation?
Hard scene discrimination	Choose the most likely scene class for this infrared image and explain why it is not a confusing alternative.
Hard-negative contrast	Describe one plausible wrong scene label for this image and explain why that label is less likely.

These prompts define the evaluation interface rather than a hidden training advantage. Each task uses the same held-out image pool and a fixed prompt template, so changes in the diagnostic metrics reflect model behavior under comparable instructions. The prompt wording is included verbatim to make later reruns sensitive to the same instruction constraints.

C.2 IR-Aware Caption Generation

The caption-rewriting prompt is included as a compact card to make the supervision recipe auditable without expanding the main text.

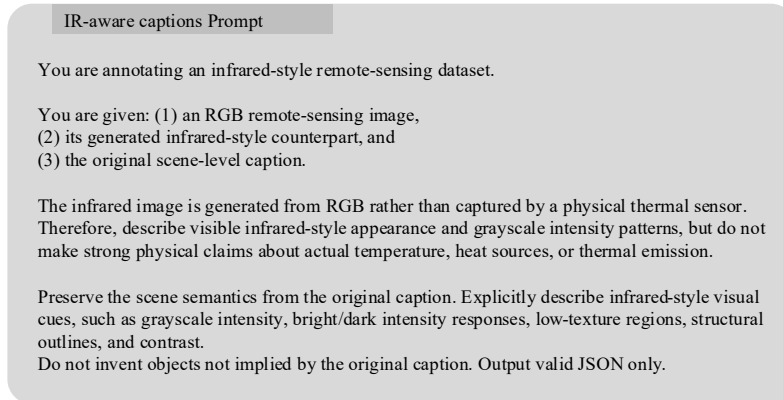


Fig. 4: Prompt card for IR-aware caption generation.

C.3 CLIP Fine-Tuning Hyperparameters

All IR-CLIP backbones are fine-tuned with a frozen text encoder, AdamW, weight decay 0.1, gradient clipping 1.0, fp16 mixed precision, and a linear-warmup (20 steps) plus cosine-decay schedule. The input resolution follows each backbone’s native CLIP processor (224²). Per-backbone settings are listed in Table 18; OpenAI ViT-L/14 additionally uses a stage-2 resume (6 epochs, lr 5×10^{-7}) from its stage-1 checkpoint.

Table 18: IR-CLIP fine-tuning hyperparameters. Batch sizes are the preferred values; the training queue automatically backs off under out-of-memory conditions.

Backbone	Epochs	Batch	LR	Text enc.
OpenAI CLIP ViT-B/32	2	768	2×10^{-6}	frozen
OpenAI CLIP ViT-L/14	2 (+6)	256 (128)	1×10^{-6} (5×10^{-7})	frozen
OpenCLIP ViT-B/32	2	1024	2×10^{-6}	frozen
GeoRSCLIP ViT-B/32	2	1024	2×10^{-6}	frozen
RemoteCLIP ViT-B/32	2	1024	2×10^{-6}	frozen

The CLIP configuration keeps the text side fixed and concentrates adaptation on the image side and projection parameters. This design makes the comparison across backbones easier to interpret because the language space is not re-learned

for each model. The extra stage-2 resume for OpenAI CLIP ViT-L/14 is reported separately because it is the only CLIP run with an extended schedule.

C.4 VLM LoRA Fine-Tuning Hyperparameters

All six IR-VLM backbones use frozen base language models and vision towers with LoRA adapters. Shared LoRA and optimizer settings are fixed across runs, while effective batch sizes and target modules differ by backbone, as summarized in Table 19.

Table 19: IR-VLM LoRA fine-tuning settings. Effective batch is per-device batch \times gradient accumulation; all runs share $r=32$, $\alpha=64$, dropout 0.05, lr 2×10^{-4} , and one epoch.

Backbone	Eff. batch	Max len	LoRA target modules
Qwen2.5-VL-7B	1×8	processor default	q,k,v,o,gate,up,down proj
InstructBLIP-FLAN-T5-XL	2×8	128	q, v
LLaVA-1.5-7B	4×4	1024	attention/MLP proj (LLaVA default)
LLaVA-1.6-Vicuna-7B	4×4	1024	attention/MLP proj (LLaVA default)
GeoChat-7B	4×4	1024	attention/MLP proj (LLaVA default)
H2RSVLM-VHM-7B	4×4	1024	attention/MLP proj (LLaVA default)

This parameter-efficient setup isolates adapter and projector adaptation while keeping the six-backbone comparison controlled.

C.5 DiffV2IR Generation Settings

Infrared images are synthesized with DiffV2IR using the `after_phase_2` checkpoint, a k-diffusion Euler-ancestral sampler, 20 steps, and 512 long-side resolution aligned to multiples of 64. Generation uses three-way classifier-free guidance with text scale 7.5, image and segmentation scales 1.5, seed 1234, and an Otsu-threshold segmentation map as the second condition. Outputs are saved as JPEG (quality 95) for all five sources and for the AVIID visible test images used in the realism study.

C.6 Realism-Metric Computation

FID uses torchvision Inception-v3 (IMAGENET1K_V1) without the classifier head, yielding 2048-dimensional pooled features. Images are converted to grayscale, replicated to three channels, resized to 299^2 , and normalized with ImageNet statistics; FID is computed over exactly 804 aligned AVIID triplets (RGB / real-IR / synthetic-IR). Histogram distances use 256 normalized intensity bins over $[0, 255]$ before computing the KL, JS, χ^2 , and intersection quantities of Appendix A.3.

D Extended Discussion

What the benchmark is designed to test. MonoIR-RS is intended to evaluate whether existing vision-language backbones can be redirected toward infrared remote-sensing evidence under a controlled data boundary. The benchmark is therefore not a general claim that synthetic imagery can replace real thermal sensors. Its narrower purpose is to isolate the language-alignment problem created by the infrared modality: images lose visible color cues, captions must stop referring to unsupported RGB appearance, and models must ground their responses in grayscale structure, intensity contrast, object-background separation, and scene layout. This scope explains why the paper evaluates both retrieval models and generative VLMs. CLIP tests whether infrared images and IR-aware captions can be aligned in a shared embedding space, while VLMs test whether instruction-following models can describe and reason about the same evidence without reverting to color-centric language.

Why IR-aware supervision matters. The central difficulty in infrared remote-sensing vision-language learning is not merely a visual domain shift. It is also a supervision shift. Captions written for visible-band images often describe color, illumination, and surface appearance that are absent or unreliable in infrared imagery. If such captions are reused without rewriting, the image encoder is asked to align grayscale intensity structure with language grounded in RGB evidence. The supervision ablation in the main paper supports this interpretation: replacing original captions with IR-aware captions raises development retrieval mean recall from 30.2% to 43.0% averaged across the five CLIP backbones. This gain indicates that the text side must describe the evidence actually visible to the model, such as intensity layout, object-background contrast, texture, and scene geometry, rather than treating infrared imagery as desaturated RGB.

How to interpret the retrieval scores. The absolute CLIP retrieval numbers remain modest even after fine-tuning, with the best model reaching 19.2% mean recall on the filtered 9,720-image test split. This should be read as evidence that the task is difficult, not as failure of the adaptation recipe. Remote-sensing scenes often contain repeated layouts, visually similar land-cover patterns, and weak object-level discriminators, and the infrared modality removes many color shortcuts used by RGB-pretrained models. The important comparison is therefore against each backbone’s own zero-shot behavior under the same candidate pool. All five CLIP backbones improve after IR-aware adaptation, with gains from +3.5 to +12.8 mean-recall points. The result shows that infrared-text alignment is learnable, while also leaving substantial headroom for future real-sensor data, larger-scale supervision, and stronger hard-negative training.

Why CLIP and VLM are evaluated separately. CLIP and VLM fine-tuning answer different questions. CLIP retrieval measures whether infrared images and IR-aware captions occupy a shared embedding space, so its main evidence is bidirectional recall on the filtered 9,720-image test split. VLM adaptation measures whether a generative model follows infrared instructions without

reverting to visible-color language or unsupported thermal claims. This requires lexical behavior diagnostics rather than a single retrieval score. For captioning, the lexical IR-cue diagnostic reaches 100% across all six backbones and RGB-color leakage falls to zero in the zero-shot comparison, but longer explanatory prompts still produce more overclaiming. This is why the paper reports task-separated diagnostics: frequent infrared wording, low color leakage, and semantic correctness are related but not identical properties.

Why synthetic infrared remains useful. The image pool is synthesized because large-scale paired infrared remote-sensing image-text data are not available at the scale required for CLIP and VLM adaptation. This choice introduces a clear boundary: the generated images should be viewed as an infrared-style training and evaluation surface, not as radiometrically calibrated sensor measurements. However, the synthetic modality is not equivalent to simple grayscale conversion. On AVIID, DiffV2IR-based synthesis is closer to real infrared than RGB-to-gray under FID and grayscale-histogram distances, and the selected IR-CLIP checkpoint also improves auxiliary paired retrieval with real-infrared queries. These checks do not prove full sensor realism, but they indicate a non-trivial infrared-style alignment signal beyond simple grayscale conversion under the reported proxy metrics.

Why RGB-IR dual-modal learning is not the main target here. The construction pipeline starts from visible remote-sensing images, but the model-facing task deliberately exposes the infrared image and IR-aware text. This choice separates the paper from RGB-IR matching or fusion benchmarks. A dual-modal objective may improve paired cross-modal retrieval, but it can also let models depend on visible-domain semantics that are not present at inference time when only infrared imagery is provided. The ablation in the main paper reflects this trade-off: joint RGB-IR diagnostic training obtains a similar IR-aware development score, yet the selected recipe prioritizes infrared-text alignment because it matches the intended model input. This does not imply that RGB-IR learning is unimportant; rather, it is a different problem with a different deployment assumption.

What the VLM diagnostics do and do not prove. The VLM diagnostics are intentionally conservative lexical checks. They verify whether generated answers mention infrared evidence, avoid visible-color leakage, avoid unsupported physical claims, and sometimes repeat a source class token. These measurements are useful because the dataset does not contain human-verified dense semantic labels for every image. They should not be interpreted as full object recognition accuracy or expert-level scene understanding. For example, a high IR-cue rate means the model uses infrared-style evidence language, while a low RGB-color rate means it avoids one common failure mode. The next step is to add human-verified answers or external semantic labels so that lexical behavior can be connected to correctness.

Limitations and future directions. The main limitations follow directly from the data construction. First, the infrared images are generated from visible

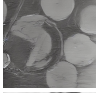
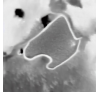

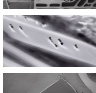
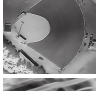
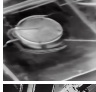


sources, so the benchmark cannot replace real sensor-captured infrared evaluation. Second, IR-aware captions and instruction answers are produced by strong foundation models and filtered automatically, which makes the supervision scalable but not equivalent to expert annotation. Third, most CLIP and VLM numbers are single-run measurements, except for the OpenAI CLIP ViT-B/32 seed check. Future work should add real infrared sensor data, radiometric metadata where available, human-verified instruction answers, larger multi-seed studies, stronger hard-negative retrieval, and semantic evaluation beyond lexical proxy metrics.

E Qualitative Case Gallery and Failure Cases

The qualitative analysis follows an extended-appendix case-table style: each example records the task setting, infrared image, prompt or query, model output, and diagnostic label. This layout makes the examples auditable rather than purely illustrative.

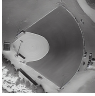
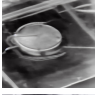
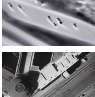
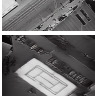
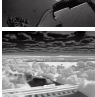



CLIP retrieval cases. For CLIP, the cases cover successful and partial retrieval, semantic near misses, and hard visual neighbors in repetitive infrared layouts. Successful examples align distinctive global geometry with IR-aware captions describing scene structure, including circular fields, runways, dense building blocks, road grids, water boundaries, and industrial tanks. Near misses arise when classes share similar infrared geometry, such as industrial areas versus dense residential blocks, river boundaries versus dark road corridors, or rail stations versus other linear transportation scenes. Because infrared imagery removes color cues and many discriminative objects occupy small regions, these examples reveal both learned alignment and residual candidate-pool ambiguity.

Table 20: Qualitative CLIP retrieval display cases. Each row restores the case-table view used for manual inspection: the held-out query image, the target caption, the retrieved evidence, and the diagnostic reading are shown together. We include eight representative cases to cover correct retrieval, partial retrieval, semantic near misses, and hard visual neighbors.

Case	Query image	Target caption	Retrieved evidence	Diagnostic
Correct top-1		Circular farmlands appear as bright rounded regions against a darker, low-texture background.	Rank 1 retrieves the paired circular-farmland caption; lower ranks contain related circular storage or industrial layouts.	Correct match at rank 1; global circular geometry is aligned.
Correct in top-5		A bright island boundary contrasts with darker surrounding water and textured vegetation.	Rank 1 is a wetland with dark water boundaries; rank 2 is the paired island caption.	Correct match appears after a visually close water-boundary neighbor.
Semantic near miss		An airport-like grid of runways and bright building regions appears against darker surroundings.	Top retrieved captions describe airport layouts with runways, taxiways, and strong grayscale contrast.	Airport semantics are retrieved, but the exact pair falls outside top-10.
Hard visual neighbor		Parking-like bright compact objects are arranged over a darker paved surface with regular boundaries.	Top evidence mixes dense built-up pavement, parking-lot captions, and industrial-yard layouts.	Repeated paved layouts create close competitors.
Baseball-field match		A baseball field is visible as a broad rounded infield and darker surrounding outfield.	Retrieved evidence describes a baseball diamond and adjacent low-texture field boundaries.	Sports-field geometry gives a stable retrieval cue.
Oil-tank match		A circular storage tank appears as a bright rounded structure beside linear road patterns.	Top captions emphasize circular tanks, industrial surfaces, and adjacent access roads.	Circular industrial objects are visually distinctive.
Rail-station neighbor		Parallel rail tracks and station-like roof structures form a dense transportation layout.	Retrieved evidence mixes train-station, bridge, and dense transport-infrastructure captions.	Linear infrastructure creates plausible near neighbors.
Reservoir boundary		A dark water body is bounded by a bright shoreline and smooth surrounding terrain.	Top evidence favors reservoir or lake captions with strong water-land contrast.	Water-boundary contrast supports alignment.

VLM generation cases. For VLMs, examples are grouped by prompt type because captioning, classification, object listing, evidence QA, cue explanation, hard-scene discrimination, hard-negative contrast, and color-leakage checking stress different behaviors. A useful response should identify the remote-sensing scene, ground the answer in visible infrared structures, and avoid importing unsupported visible-color descriptions. The successful cases typically mention grayscale contrast, bright-dark boundaries, compact object arrangements, linear transportation structures, or water-land separation as evidence. The more difficult cases test whether the model can distinguish visually similar layouts, such as airports versus roads, rail stations versus other dense infrastructure, bridges versus linear banks, or reservoirs versus dark background regions. These examples therefore complement the quantitative diagnostics by showing whether the generated answers are concise, visually grounded, and consistent with the intended modality.

Table 21: Qualitative VLM generation display cases. Each row shows the held-out image, the evaluation prompt, the generated answer, and the manual diagnostic label used when preparing the case gallery. We include eight prompt types to show concise captioning, classification, object listing, evidence-grounded QA, cue explanation, hard-scene discrimination, hard-negative contrast, and color-leakage checking.

Task	Image	Prompt	Generated answer	Diagnostic
Captioning		Describe this infrared image in one sentence.	A baseball field shows a bright infield, darker outfield, and low-texture surroundings.	Concise scene grounding.
Scene classification		Classify the scene and give one visual reason.	Industrial area; circular tank structure visible in grayscale.	Class plus visual reason.
Infrared-cue explanation		Explain the infrared visual cues.	High-contrast outlines and grayscale intensity variation reveal parked cars against darker pavement.	Uses intensity cues.
Hard-negative contrast		Give a wrong label and explain why.	Airport; dense buildings and railway tracks are visible, while runways or terminals are absent.	Rejects confusing label.
Object presence		List the main visible objects or land-cover elements.	Tennis courts, paved surfaces, nearby buildings, and dark boundary regions are visible.	Object list grounded in structure.
Visual-evidence QA		What visible infrared evidence supports the scene interpretation?	The bright bridge deck, dark water channel, and repeated linear supports indicate a bridge scene.	Uses local visual evidence.
Hard scene discrimination		Choose the most likely scene class and explain why it is not a confusing alternative.	Airport; the long runway-like strip and open surrounding area are more consistent than a road.	Distinguishes similar linear scenes.
Color-leakage check		Describe the image without using visible-color terms.	A dark reservoir occupies the center, bordered by bright shoreline and smoother surrounding terrain.	Avoids RGB-color wording.